Turk J Pharm Sci
DOI: 10.4274/tjps.galenos.2026.47564

ORIGINAL ARTICLE

N-Benzyl Indole-Benzoxazole Hybrids as Multi-Target Anticancer Agents Modulating mTOR, Apoptosis, and Lipid Dynamics in Breast Cancer

Burak KUZU[1]*, Eda AÇIKGÖZ[2], Mustafa ÇAKIR[3]

[1]Van Yüzüncü Yıl University Faculty of Pharmacy, Department of Pharmaceutical Chemistry, Van, Türkiye
[2]Van Yüzüncü Yıl University Faculty of Medicine, Department of Histology and Embryology, Van, Türkiye
[3]Van Yüzüncü Yıl University Faculty of Medicine, Department of Medical Biology, Van, Türkiye

ABSTRACT

Objectives: Indole-benzoxazole hybrids are structurally versatile scaffolds with significant promise in anticancer drug development. This study aimed to synthesize N-benzyl-substituted indole-benzoxazole derivatives (IBB1-5) and to evaluate their antiproliferative potential and mechanistic effects in human breast cancer models.

Materials and Methods: IBB1-5 were synthesized and screened for cytotoxic activity against MDA-MB-231 and MCF-7 cells using MTT assays. The most active compound, IBB-4, was further investigated in MDA-MB-231 cells through clonogenic assays and morphological analysis. Immunofluorescence staining was performed to assess mTOR, LC3, caspase-3, and β-tubulin expression and distribution. Lipid droplet dynamics were evaluated using Oil Red O and Nile Red staining, combined with three-dimensional surface-plot analysis.

Results: IBB-4 demonstrated the strongest growth-inhibitory activity, with IC_{50} values of 12.2 μM (MDA-MB-231) and 12.8 μM (MCF-7). Clonogenic assays revealed significant dose-dependent suppression of long-term proliferative capacity. Morphological alterations included cytoplasmic vacuolization and structural disorganization. Immunofluorescence analyses showed a marked downregulation of mTOR and a spatial redistribution of LC3, without significant changes in total fluorescence intensity. Increased caspase-3 immunoreactivity and pronounced disruption of β-tubulin indicated activation of apoptotic pathways and cytoskeletal destabilization. Lipid staining, supported by three-dimensional surface analysis, demonstrated prominent clustering and redistribution of intracellular lipid droplets.

Conclusion: IBB-4 exerts multi-layered anticancer effects through coordinated modulation of proliferative signaling, apoptotic activation, cytoskeletal integrity, and lipid compartmentalization. These findings identify IBB-4 as a promising lead candidate for further molecular and preclinical investigations, particularly in triple-negative breast cancer.

Keywords: Indole-benzoxazole hybrids, breast cancer, mTOR, apoptosis, lipid metabolism, anticancer activity

INTRODUCTION

Breast cancer is a heterogeneous malignant neoplasm arising from mammary epithelial tissue and is the most commonly diagnosed cancer among women worldwide, posing a significant global public health challenge.[1] A recent analysis by the International Agency for Research on Cancer estimates that the global impact of breast cancer will rise significantly by 2050, with projected increases of approximately 38% in incidence and 68% in mortality, largely driven by population growth, population aging, and lifestyle-related risk factors.[2] These alarming projections underscore the escalating public health challenge posed by breast cancer and highlight the urgent need for improved preventive, diagnostic, and therapeutic strategies.

***Correspondence:** burakkuzu@yyu.edu.tr, **ORCID-ID:** orcid.org/0000-0002-7305-7177

Received: 27.02.2026 **Accepted:** 23.10.2026 **Epub:** 06.11.2026

Cite this article as: Kuzu B, Açıkgöz E, Çakır M. N-benzyl indole-benzoxazole hybrids as multi-target anticancer agents modulating mTOR, apoptosis, and lipid dynamics in breast cancer. Turk J Pharm Sci. [Epub Ahead of Print]

Copyright© 2026 The Author(s). Published by Galenos Publishing House on behalf of Turkish Pharmacists' Association.
This is an open access article under the Creative Commons Attribution-NonCommercial-NoDerivatives 4.0 (CC BY-NC-ND) International License.

In addition, invasive and metastatic behaviors vary substantially among breast cancer subtypes. Breast cancer comprises a biologically diverse group of tumors that can be stratified based on histopathological features, genetic alterations, and molecular aberrations.[3] Progress in gene expression profiling has enabled the classification of breast cancer into distinct molecular subtypes: luminal A, luminal B, human epidermal growth factor receptor 2 (HER2)-enriched, basal-like, and triple-negative breast cancer (TNBC).[4] These classifications have provided a more precise framework for understanding tumor biology and have significantly contributed to the development of subtype-specific therapeutic strategies. In particular, TNBC has garnered significant attention owing to its aggressive phenotype, high metastatic potential, and poor clinical prognosis.[5]

Despite substantial advances in breast cancer management, including endocrine therapy, HER2-targeted agents, chemotherapy, and more recently immunotherapeutic approaches, therapeutic resistance and disease recurrence remain significant clinical challenges.[6] These limitations are particularly pronounced in aggressive subtypes such as TNBC, where the absence of well-defined molecular targets restricts treatment options largely to cytotoxic chemotherapy. Consequently, the identification and development of novel small-molecule agents with improved selectivity, multi-target potential, and enhanced antiproliferative efficacy represent a critical focus in contemporary anticancer drug discovery.[7] In this context, owing to their architectural flexibility and diverse pharmacological properties, heterocyclic moieties have become fundamental scaffolds in drug discovery. Accumulating evidence indicates that indole- and benzoxazole-based compounds exhibit notable anticancer activity, largely due to their ability to modulate key oncogenic signaling pathways that regulate cell proliferation, apoptosis, and metastatic progression.[8-10] The rational hybridization of these two bioactive pharmacophores offers a promising strategy for generating novel therapeutic candidates with enhanced biological performance.

In line with the growing interest in indole- and benzoxazole-based scaffolds, several structurally diverse derivatives have been reported to exhibit significant antiproliferative activity against breast cancer cell lines. For example, the carbohydrazide-substituted indole derivative 1 exhibited significant cytotoxicity against MCF-7 cells (IC_{50} = 24.6 ± 0.33 μg/mL) and demonstrated notable affinity for CDK4, suggesting a cell-cycle–related antiproliferative mechanism.[11] Sulfonohydrazide derivative 2, bearing indole and morpholine heterocycles, showed potent and selective activity in MCF-7 and MDA-MB-468 cells (IC_{50} = 13.2 and 8.2 μM, respectively).[12] The indole–benzimidazole hybrid 3 exhibited marked antiproliferative effects in ER-α-positive T47D cells by modulating ER-α and exerting SERM-like antagonism.[13] Among benzoxazole derivatives, compound 4 demonstrated strong antiproliferative activity (IC_{50} = 4.96-9.82 μM) and inhibited mTOR phosphorylation (Ser2448) while promoting apoptosis via regulation of Bax, caspase-3, p53, and Bcl-2.[14] Pyrrole-substituted benzoxazole derivative 5 exhibited selective cytotoxicity toward MCF-7 cells (IC_{50} = 4.29 μM).[15] In contrast, pyrrole-tethered bisbenzoxazole derivatives 6 showed pronounced activity with approximately eightfold greater potency than tamoxifen, inducing G1 arrest and caspase-9-mediated apoptosis with minimal toxicity toward healthy fibroblasts (Figure 1).[16] Collectively, these findings underscore the therapeutic promise of indole and benzoxazole frameworks for breast cancer. Despite their significant biological activities, structurally integrated hybrid systems that simultaneously exploit multiple mechanistic pathways remain comparatively underexplored, underscoring the need for novel molecular architectures with enhanced multitarget potential.

In breast cancer, metabolic reprogramming is now recognized as a defining hallmark of tumor progression, with lipid metabolism occupying a central position in sustaining rapid proliferation, membrane biogenesis, redox balance, and therapy resistance.[17] Increased *de novo* lipogenesis, dysregulated cholesterol homeostasis, and dynamic remodeling of lipid droplets collectively contribute to tumor aggressiveness and adaptive survival.[18] Importantly, the mTOR-autophagy axis functions not only as a master regulator of growth signaling but also as a critical integrator of metabolic control, directly coordinating lipid biosynthesis and autophagic flux.[19] Thus, pharmacological modulation of this pathway may simultaneously disrupt proliferative and metabolic circuits within cancer cells. Beyond oncology, benzoxazole derivatives have been reported to attenuate high-fat diet-induced hyperlipidemia by modulating lipid-regulating genes, suggesting that this scaffold may harbor intrinsic metabolic regulatory capacity that extends beyond conventional cytotoxic mechanisms.[20] This dual biological relevance positions benzoxazole-based compounds as attractive candidates for targeting interconnected survival and metabolic pathways in breast cancer.

Accordingly, the current investigation aimed to comprehensively evaluate the anticancer potential of newly synthesized indole-benzoxazole hybrids, rationally constructed by integrating an indole pharmacophore known to target breast cancer cells, a substituted benzoxazole unit aimed at mTOR inhibition, and an N-benzyl moiety to enhance efficacy against breast cancer (Figure 2). This design strategy enables a multifaceted approach, allowing the investigation of mTOR signaling, autophagic regulation (LC3), apoptotic execution (caspase-3), and lipid-associated cellular alterations within breast cancer

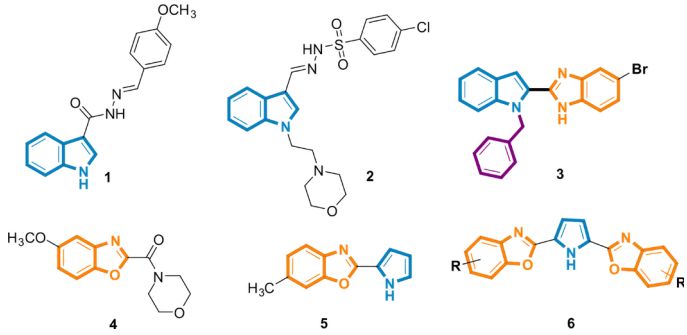


Figure 1. Representative indole- and benzoxazole-based derivatives reported in the literature exhibit antiproliferative activity against various breast cancer cell lines.

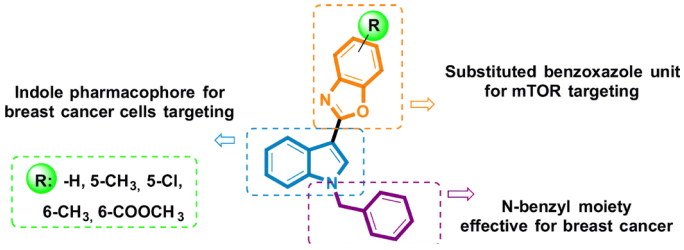


Figure 2. Structural framework of indole-benzoxazole hybrids highlighting key pharmacophores for breast cancer targeting and mTOR inhibition.

models. By simultaneously interrogating survival pathways and metabolic reprogramming, we aim to elucidate the mechanistic scope and therapeutic relevance of these novel derivatives.

MATERIALS AND METHODS

Chemistry

General

All reagents and solvents were used as received from commercial suppliers. ^{1}H-NMR and ^{13}C-NMR spectra were recorded on a Varian-Agilent Inova spectrometer (400 MHz and 100 MHz, respectively) with TMS as the internal standard. Melting points were determined in open capillaries using a Stuart SMP30 apparatus (uncorrected). High-resolution mass spectrometry (HRMS) analyses were performed on a THERMO ITQ900 spectrometer equipped with an ESI source. Reported yields correspond to analytically pure, isolated products.

Synthesis of the carbaldehyde-substituted indole

Indole (2 mmol) was dissolved in 4 mL of anhydrous N, N-dimethylformamide (DMF) and cooled to 0 °C in an ice bath. Phosphorus oxychloride was then added dropwise to generate the Vilsmeier reagent *in situ*. The mixture was stirred at 0 °C for 1 hour to allow complete formation of the electrophilic intermediate and then heated to 90 °C under reflux for 12–16 hours to achieve formylation of the indole ring. Reaction progress was monitored by thin-layer chromatography (TLC). After completion, the mixture was carefully poured into 50 mL of ice water to quench the reaction and precipitate the product. The solid was collected by vacuum filtration, washed with cold water, and dried at room temperature. The resulting crude carbaldehyde-substituted indole was isolated as a solid and used directly in subsequent reactions without further purification.[21]

Synthesis of N-substituted indole-3-carbaldehyde derivatives

N-benzyl-indole-3-carbaldehyde was synthesized via N-benzylation of indole-3-carbaldehyde with benzyl bromide. In a typical procedure, indole-3-carbaldehyde (1 equiv) was dissolved in 10 mL of anhydrous DMF at room temperature, and the resulting solution was cooled to 0 °C in an ice bath. Sodium hydride (NaH, 2 equiv) was added portionwise with stirring at 0 °C, and the mixture was maintained at this temperature for 45 minutes to generate the indole anion. Subsequently, benzyl bromide (1.2 equiv) was added dropwise, and the reaction progress was monitored by TLC. Upon completion of the reaction (approximately 2 hours), the mixture was quenched by pouring into ice-cold water to precipitate the product. The resulting solid was collected by filtration, washed thoroughly with water to remove residual salts, and recrystallized from diethyl ether to afford the target N-benzylated indole-3-carbaldehyde structures in high yields.[22]

Synthesis of indole-(2-aminophenol) Schiff bases

Carbaldehyde-substituted indole (1 mmol) was dissolved in 10 mL of ethanol. To this solution, o-aminophenol derivatives (1 mmol) dissolved in 7 mL of ethanol were added, followed by acetic acid (0.4 mL) as a co-reactant. The reaction mixture was stirred; upon completion, the solvent was removed under vacuum, and the resulting residue was poured into an ice-water mixture to precipitate the Schiff base. The solid product was collected by filtration and dried under ambient conditions. The obtained Schiff bases were used directly in subsequent reactions without further purification.[15]

Synthesis of target indole-benzoxazole hybrid derivatives

The Schiff base intermediates obtained in the previous step were dissolved in 5 mL of anhydrous DMF. 0.1 g of sodium cyanide (NaCN) was added, and the reaction mixture was allowed to stand at room temperature for 12 hours. Upon completion, 0.2 mL of hydrogen peroxide (H_2O_2) was introduced, and stirring was continued for an additional hour to facilitate oxidative cyclization. The reaction medium was subsequently quenched and extracted with a saturated salt solution (15 mL) and ethyl acetate (3 × 10 mL). The combined organic layers were dried, and the solvent was evaporated under reduced pressure to yield the crude product. Final purification of the target indole-benzoxazole hybrids was achieved by column chromatography using appropriate ratios of ethyl acetate to n-hexane as the mobile phase, affording the pure compounds.[23]

Characterization data of target indole-benzoxazole hybrid derivatives

2-(1-benzyl-1H-indol-3-yl) benzo[d]oxazole (IBB-1)

Light brown solid, M.p.: 95.1-95.3 °C, Yield: 68%. ^{1}H-NMR (400 MHz, $CDCl_3$) δ 8.49 (d, *J* = 7.8 Hz, 1H, Ar-H), 8.06 (s, 1H, Ar-H), 7.73 (dd, *J* = 1.4 Hz, *J* = 7.1 Hz, 1H, Ar-H), 7.54 (d, *J* = 7.8 Hz, 1H, Ar-H), 7.38-7.26 (m, 8H, Ar-H), 7.20 (d, *J* = 7.3 Hz, 2H, Ar-H), 5.38 (s, 2H, -CH_2-). ^{13}C-NMR (100 MHz, $CDCl_3$) δ 161.2, 149.8, 136.9, 135.9, 131.4, 129.0, 128.2, 127.2, 125.9, 124.3, 123.9, 123.3, 122.0, 121.8, 118.9, 110.4, 110.0, 104.0, 50.8. HRMS $[M+H]^+$: calculated for $C_{22}H_{17}N_2O$: 325.1335, found: 325.1340.

2-(1-benzyl-1H-indol-3-yl)-5-methylbenzo[d]oxazole (IBB-2)

Light gray solid, M.p.: 119.3-119.9 °C, Yield: 71%. ^{1}H-NMR (400 MHz, $CDCl_3$) δ 8.48 (d, *J* = 7.8 Hz, 1H, Ar-H), 8.00 (s, 1H, Ar-H), 7.51 (bs, 1H, Ar-H), 7.40 (d, *J* = 8.2 Hz, 1H, Ar-H), 7.37-7.27 (m, 6H, Ar-H), 7.19 (d, *J* = 7.4 Hz, 2H, Ar-H), 7.08 (d, *J* = 8.2 Hz, 1H, Ar-H), 5.36 (s, 2H, -CH_2-), 2.47 (s, 3H, Ar-CH_3). ^{13}C-NMR (100 MHz, $CDCl_3$) δ 161.3, 148.0, 142.3, 136.8, 136.0, 133.9, 131.1, 129.0, 128.1, 127.2, 125.9, 124.9, 123.3, 121.9, 121.8, 119.0, 110.4, 109.3, 104.3, 50.7, 21.6. HRMS $[M+H]^+$: calculated for $C_{23}H_{19}N_2O$: 339.1491, found: 339.1499.

2-(1-benzyl-1H-indol-3-yl)-5-chlorobenzo[d]oxazole (IBB-3)

Light orange solid, M.p.: 131.8-132.4 °C, Yield: 75%. ^{1}H-NMR (400 MHz, $CDCl_3$) δ 8.45 (d, *J* = 8.2 Hz, 1H, Ar-H), 7.99 (s, 1H, Ar-H), 7.68 (d, *J* = 2.0 Hz, 1H, Ar-H), 7.42 (d, *J* = 8.2 Hz, 1H, Ar-H), 7.38-7.28 (m, 6H, Ar-H), 7.24-7.19 (m, 3H, Ar-H), 5.38 (s, 2H, -CH_2-). ^{13}C-NMR (100 MHz, $CDCl_3$) δ 162.5, 148.4, 143.5, 136.9, 135.7, 131.6, 129.6, 129.0, 128.2, 127.2, 125.8, 123.9, 123.5, 122.2, 121.7, 118.9, 110.6, 110.5, 103.7, 50.8. HRMS $[M+H]^+$: calculated for $C_{22}H_{16}ClN_2O$: 359.0945, found: 359.0950; $[M+H+2]^+$: 361.0916, found: 361.0919.

2-(1-benzyl-1H-indol-3-yl)-6-methylbenzo[d]oxazole (IBB-4)

White solid, M.p.: 154.2-154.8 °C, Yield: 66%. ^{1}H-NMR (400 MHz, $CDCl_3$) δ 8.47 (d, *J* = 8.0 Hz, 1H, Ar-H), 8.00 (s, 1H, Ar-H), 7.59 (d, *J* = 8.0 Hz, 1H, Ar-H), 7.38-7.27 (m, 7H, Ar-H), 7.24-7.16 (m, 2H, Ar-H), 7.12 (d, *J* = 8.0 Hz, 1H, Ar-H), 5.38 (s, 2H, -CH_2-), 2.49 (s, 3H, Ar-CH_3). ^{13}C-NMR (100 MHz, $CDCl_3$) δ 160.7, 150.0, 136.8, 135.9, 134.3, 131.3, 129.0, 128.2, 127.2, 125.8, 125.4, 123.3, 121.9, 121.8, 118.1, 110.4, 110.3, 50.8, 21.8. HRMS $[M+H]^+$: calculated for $C_{23}H_{19}N_2O$: 339.1491, found: 339.1496.

Methyl 2-(1-benzyl-1H-indol-3-yl) benzo[d]oxazole-6-carboxylate (IBB-5)

Light brown solid, M.p.: 190.4-190.8 °C, yield: 73%. ^{1}H-NMR (400 MHz, $CDCl_3$) δ 8.47 (d, *J* = 8.1 Hz, 1H, Ar-H), 8.20 (s, 1H, Ar-H), 8.08-8.01 (m, 2H, Ar-H), 7.71 (d, *J* = 8.1 Hz, 1H, Ar-H), 7.39-7.29 (m, 6H, Ar-H), 7.21-7.17 (m, 2H, Ar-H), 5.38 (s, 2H, -CH_2-), 3.94 (s, 3H, -$COOCH_3$). ^{13}C-NMR (100 MHz, $CDCl_3$) δ 166.9, 164.0, 149.5, 146.5, 136.9, 136.7, 132.0, 129.1, 128.3, 127.2, 126.3, 125.8, 125.7, 123.5, 122.3, 121.8, 118.3, 111.5, 110.5, 103.7, 52.3, 50.9. HRMS $[M+H]^+$: calculated for $C_{24}H_{19}N_2O_3$: 383.1390, found: 383.1394.

Cell culture

The MCF-7 (estrogen receptor-positive; ATCC® HTB-22™) and MDA-MB-231 (estrogen receptor-negative; ATCC® HTB-26™) breast cancer cell lines were obtained from ATCC (USA). Cells were cultured in DMEM supplemented with 10% FBS, 100 U/mL penicillin, 100 µg/mL streptomycin, and amphotericin B, and maintained at 37 °C in a humidified incubator with 5% CO_2. Subculturing was performed at 70–80% confluency using standard trypsinization procedures.

Cell proliferation assay

Stock solutions of IBB-1 to IBB-5 were prepared in dimethyl sulfoxide (DMSO) and diluted with culture medium to achieve the desired working concentrations. The final DMSO concentration in all treatments, including controls, was maintained at ≤ 0.1% (v/v). MDA-MB-231 cells were seeded in 96-well plates and allowed to adhere overnight and were then exposed to increasing concentrations of the IBB compounds for the specified duration. After treatment, cell viability was determined using the MTT assay following standard procedures. Absorbance was recorded at 570 nm with a microplate reader, and viability was calculated relative to the vehicle-treated control.

Colony formation assay

MDA-MB-231 cells were seeded at low density (1,000–1,500 cells per well) in 6-well plates and allowed to adhere overnight. Cells were treated with IBB-1 through IBB-5; IBB-4 was applied at 6, 12, and 18 µM as specified. Following treatment, the medium was replaced with fresh drug-free medium, and cells were incubated for 7–8 days to permit colony formation. Colonies were then fixed with paraformaldehyde, stained with crystal violet, and counted manually. Colony counts were normalized to the control group and expressed as a percentage of the control group.

Hematoxylin-eosin staining

Morphological changes in MDA-MB-231 cells were assessed using hematoxylin-eosin staining. Cells were fixed with 4% paraformaldehyde for 15 min at room temperature and washed with phosphate-buffered saline (PBS). Fixation was followed by sequential staining with hematoxylin for 1 min and eosin for 30 s. Excess stain was removed by gentle PBS washes, and the cells were mounted in a suitable mounting medium. Morphological alterations associated with treatment were examined under a light microscope.

Immunofluorescence staining

MDA-MB-231 cells were seeded on glass coverslips and allowed to adhere under standard culture conditions prior to treatment with IBB-4. After treatment, cells were fixed with 4% paraformaldehyde for 15 min at room temperature, washed with PBS, and permeabilized with 0.025% Triton X-100 for 10 min. Non-specific binding was blocked with PBS containing BSA for 1 h at room temperature. Cells were then incubated overnight at 4 °C with primary antibodies against mTOR (bs-1992R, Bioss), LC3 (bs-8878R, Bioss), caspase-3 (#9661, Cell Signaling), and β-tubulin (#2146S, Cell Signaling) at 1:200 dilution. After washing, cells were incubated with FITC-conjugated secondary antibodies for 1 h at room temperature in a humidified, light-protected chamber, followed by thorough PBS washes. Coverslips were mounted using a DAPI-containing medium and examined with an Olympus BX53 fluorescence microscope equipped with a DP74 camera. Images were captured under consistent exposure settings, and fluorescence intensity was quantified using ImageJ (NIH, Bethesda, MD). For each condition, 50 randomly selected cells were analyzed for comparative assessment.

Oil red O (ORO) staining

Intracellular lipid accumulation in MDA-MB-231 cells was assessed using ORO staining. Cells were seeded on glass coverslips and cultured under standard conditions until attachment was achieved. Cells were fixed with 4% paraformaldehyde for 15 min at room temperature, rinsed with distilled water, and equilibrated in 60% isopropanol. The ORO working solution was freshly prepared by diluting a 3 mg/mL stock solution with deionized water (3:2 v/v), homogenizing and filtering before use. Cells were incubated with ORO for 10–15 min at room temperature and then counterstained with hematoxylin for 1 min. After thorough washing with distilled water, coverslips were mounted in cell-mounting medium and examined by light microscopy to qualitatively assess intracellular lipid droplets.

Nile red staining

Intracellular lipid droplets in MDA-MB-231 cells were visualized using Nile red staining. Treated cells were fixed with 4% paraformaldehyde for 15 min at room temperature and washed with PBS. Cells were incubated in the dark for 15 min with Nile red (0.1 µg/mL in 150 mM sodium chloride). After washing to remove excess dye, coverslips were mounted with a DAPI-containing medium, and fluorescence images were acquired using an Olympus BX53 microscope.

Statistical analysis

All statistical analyses were conducted using GraphPad Prism 9.5 (GraphPad Software, San Diego, CA, USA). One-way analysis of variance (ANOVA) followed by Tukey's multiple comparisons test was applied to cell viability and apoptosis assays. Cell cycle distributions were analyzed using one-way ANOVA with Dunnett's post-hoc test, comparing each treatment to the control. IC_{50} values and 95% confidence intervals were determined via non-linear regression. A p-value < 0.05 was considered statistically significant. Significance levels are denoted as: *$p < 0.05$; **$p < 0.01$; ***$p < 0.001$; ****$p < 0.0001$.

RESULTS

Chemistry

The target indole-benzoxazole hybrids were synthesized through a concise four-step sequence, as outlined in Figure 3. To the best of our knowledge, all synthesized IBB1-5 derivatives are novel compounds that have not been previously reported in the literature. Initially, carbaldehyde-substituted indole derivatives were obtained via Vilsmeier formylation of the corresponding indole scaffolds. Subsequent N-alkylation with benzyl bromide derivatives yielded the N-substituted indole-3-carbaldehyde intermediates. These intermediates were then condensed with 2-aminophenol derivatives under mild acidic conditions to furnish the corresponding Schiff bases. Finally, oxidative cyclization of the Schiff bases in the presence of catalytic NaCN and H_2O_2 afforded the desired indole-benzoxazole hybrids.

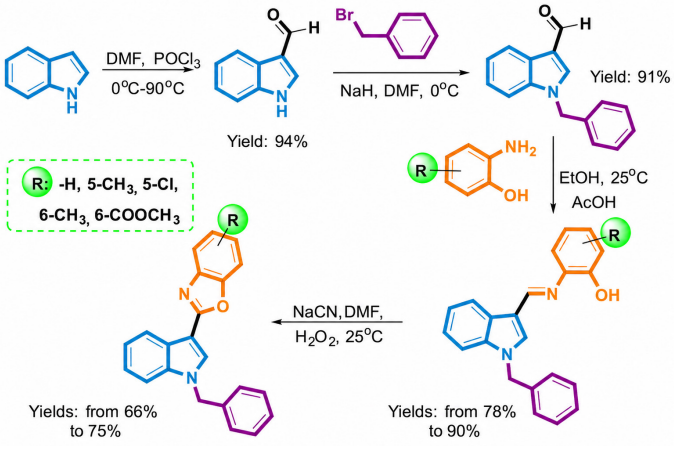


Figure 3. General synthesis scheme for target N-benzyl substituted indole-benzoxazole hybrids.

DMF, N, N-dimethylformamide; $POCl_3$, phosphorus oxychloride; NaH, sodium hydride; EtOH, ethanol; AcOH, acetic acid; NaCN, sodium cyanide; H_2O_2, hydrogen peroxide.

Following the successful synthesis, the target indole-benzoxazole hybrids (IBB-1-IBB-5) were obtained in moderate-to-good yields (66–75%) as crystalline solids, with melting points ranging from 95 to 190 °C. Structural characterization was performed using ^{1}H and ^{13}C-NMR spectroscopy, which confirmed the expected frameworks. In the ^{1}H-NMR spectra, the methylene protons of the N-benzyl substituent consistently appeared as singlets at δ 5.36-5.38 ppm, while aromatic protons were observed between δ 7.1–8.5 ppm, reflecting the indole and benzoxazole environments. The ^{13}C-NMR spectra provided further confirmation, showing characteristic signals for the benzoxazole carbonyl and aromatic carbons (δ 104-166 ppm), as well as the methylene linker (δ 50-51 ppm). Substituent effects were clearly evident: methyl or chloro groups on the benzoxazole ring induced predictable chemical shift variations in both ^{1}H and ^{13}C spectra. HRMS analysis corroborated the molecular formulas, with observed $[M+H]^+$ values in excellent agreement with calculated masses. Collectively, the consistent NMR patterns, HRMS confirmation, and satisfactory isolated yields demonstrate the efficiency and reliability of the four-step synthetic strategy, providing a robust foundation for subsequent biological evaluation. The NMR and HRMS spectra of the synthesized compounds are provided in the Supplementary Material.

Cytotoxic activity and structure-activity relationship analysis of compounds IBB1-5 in MDA-MB-231 and MCF-7 breast cancer cells

The cytotoxic activities of compounds IBB1-5 were evaluated against the human breast cancer cell lines MDA-MB-231 and MCF-7 following 72 h of treatment. The compounds showed distinct cytotoxic profiles, with IC_{50} values ranging from 12.2 to 47.6 µM in MDA-MB-231 cells and from 12.4 to 50.3 µM in MCF-7 cells (Table 1). IBB-4 was the most potent compound against MDA-MB-231 cells (IC_{50} = 12.2 µM), whereas IBB-3 showed the highest activity against MCF-7 cells (IC_{50} = 12.4 µM). Notably, IBB-4 also retained high activity in MCF-7 cells, with an IC_{50} value of 12.8 µM. IBB-5 showed moderate activity, with IC_{50} values of 21.2 and 14.1 µM against MDA-MB-231 and MCF-7 cells, respectively. In contrast, IBB-1 and IBB-2 were the least active compounds in the series. IBB-1 exhibited IC_{50} values of

Table 1. Cytotoxic activity of compounds IBB1-5 against human breast cancer cell lines MDA-MB-231 and MCF-7.

Compounds	IC_{50} (µM, 72 h)	
	MDA-MB-231	MCF-7
IBB-1	44.9	50.3
IBB-2	47.6	40.2
IBB-3	17.1	12.4
IBB-4	12.2	12.8
IBB-5	21.2	14.1

IBB, indole-benzoxazole derivatives.

44.9 and 50.3 µM, while IBB-2 showed values of 47.6 and 40.2 µM in MDA-MB-231 and MCF-7 cells, respectively. Accordingly, the activity order was IBB-4 > IBB-3 > IBB-5 > IBB-1 ≈ IBB-2 in MDA-MB-231 cells and IBB-3 > IBB-4 > IBB-5 > IBB-2 > IBB-1 in MCF-7 cells.

The observed activity differences provide useful information on the structural features contributing to cytotoxicity within the IBB series. All five compounds contain the same heteroaromatic core and N-benzyl substituent, while the substituent on the additional aromatic ring varies in nature and position. The most striking difference is seen between the methyl-substituted derivatives IBB-2 and IBB-4. Although these compounds differ only in the position of the methyl group, their cytotoxic profiles vary markedly. IBB-2 showed relatively weak activity in both cell lines, whereas IBB-4 was the most potent compound against MDA-MB-231 cells and remained highly active against MCF-7 cells. This isomeric difference suggests that the position of the methyl group has a substantial effect on activity, potentially by altering the molecular conformation, steric environment, or interactions of the molecule with its biological target. IBB-3, bearing a chloro substituent, also showed strong activity against both cell lines. Its considerably higher potency compared with the unsubstituted analogue IBB-1 suggests that the chlorine substituent contributes favorably to the biological profile of the series. The presence of chlorine can modify both the lipophilic and electronic properties of the molecule, which may facilitate favorable hydrophobic and other non-covalent interactions with biological targets. The activity of IBB-3, therefore, highlights halogen substitution as a useful approach to improving cytotoxic potency within this scaffold. The ester-containing derivative IBB-5 also displayed appreciable activity, with IC_{50} values lower than those of IBB-1 and IBB-2 in both cell lines. Introducing the ester group increases the molecule's hydrogen-bond-accepting capacity and alters its polarity, which may contribute to its interaction with relevant biological targets. However, IBB-5 was less potent than IBB-3 and IBB-4, indicating that the ester substituent does not provide the same favorable balance of steric, electronic, and lipophilic properties as observed with chloro and methyl substituents.

In sum, the results indicate that both the nature and position of the aromatic substituent play an important role in determining the cytotoxic activity of the IBB derivatives. The pronounced difference between the methyl-substituted isomers IBB-2 and IBB-4 particularly underscores the importance of substituent positioning, while the activity of IBB-3 suggests that chloro substitution contributes favorably. Among the tested compounds, IBB-4 stood out for having the highest potency against MDA-MB-231 cells and for exhibiting similarly strong activity against MCF-7 cells. Based on these results, IBB-4 was selected for subsequent studies to investigate its effects on cellular proliferation and clonogenic survival in MDA-MB-231 cells.

IBB-4 inhibits proliferation and clonogenic survival in MDA-MB-231 cells

IBB-4 treatment significantly suppressed proliferation of MDA-MB-231 TNBC cells in a dose-dependent manner, as demonstrated by the MTT assay (Figure 4a). The IC_{50} value was 12 µM (Figure 4b). Consistent with this finding, clonogenic survival was significantly reduced following exposure to increasing concentrations of IBB-4, indicating a substantial impairment of long-term proliferative and colony-forming capacity (Figure 4c and d). While short-term viability tests reflect acute cytotoxic or cytostatic effects, colony-forming tests provide insight into sustained tumor-initiating potential. The significant decrease in both parameters demonstrates that IBB-4 not only limits immediate cell growth but also compromises the ability of aggressive breast cancer cells to survive and re-proliferate over time. In particular, the strong inhibition observed at relatively low micromolar concentrations highlights the efficacy of IBB-4 in MDA-MB-231 TNBC, which is known for its treatment resistance and high metastatic potential. These findings are broadly consistent with previous reports indicating that small-molecule anticancer agents can reduce both short-term viability and long-term clonogenic survival in TNBC models, including MDA-MB-231 cells.[24] Concurrent decreases in metabolic activity and colony-forming capacity are generally interpreted as reflecting a more sustained growth-inhibitory effect rather than a purely transient cytostatic response.[25] Therefore, the congruent inhibition observed in both assays in this study supports the biological relevance of IBB-4's anti-tumor activity. While the molecular targets of IBB-4 have not yet been identified, the magnitude and consistency

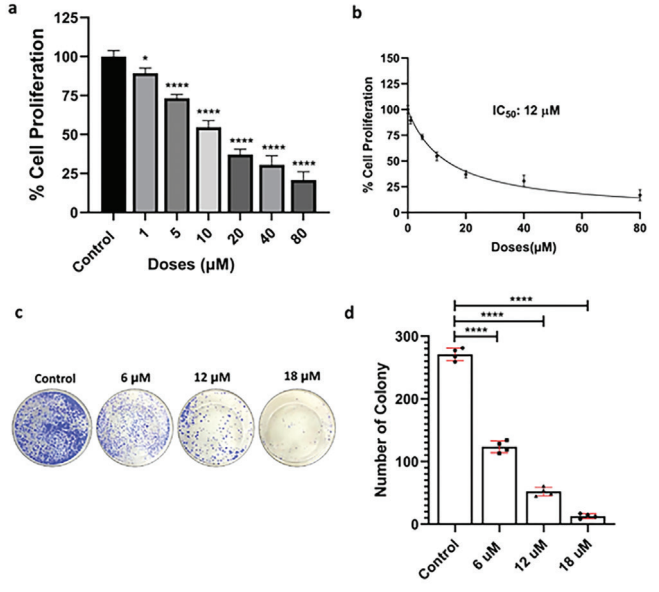


Figure 4. The compound exhibited dose-dependent antiproliferative and clonogenic inhibitory effects on MDA-MB-231 cells. (a) MTT assay results showing the effect of increasing concentrations of the compound (1-80 µM) on cell proliferation after treatment, expressed as a percentage of the control. (b) Dose-response curve derived from the MTT assay, with an IC_{50} value of 12 µM. (c) Representative images of the colony formation assay show reduced clonogenic capacity of MDA-MB-231 cells following treatment at 6, 12, and 18 µM compared with the control. (d) Quantitative analysis of colony numbers demonstrates a significant dose-dependent decrease in colony formation. Data are presented as mean ± SEM (n = 3). Statistical significance was determined relative to the control (*$p < 0.05$, ****$p < 0.0001$).

of its effects position IBB-4 as a promising compound for further mechanistic investigation and preclinical evaluation in aggressive breast cancer models.

IBB-4 treatment induces marked morphological alterations in MDA-MB-231 cells

Drug-induced morphological changes in cancer cells provide important preliminary information on cytotoxicity and potential mechanisms of cell death.[26] Therefore, cellular morphology was evaluated using light microscopy following IBB-4 treatment. Control MDA-MB-231 cells exhibited a typical adherent morphology with intact cellular architecture and uniform distribution (Figure 5). In contrast, IBB-4-treated cells showed pronounced morphological alterations. Cell adhesion decreased, and a considerable number of cells detached from the culture surface. Treated cells appeared enlarged and swollen compared to the controls. Additionally, vacuole-like structures of varying sizes were evident within the cytoplasm (Figure 5A). Hematoxylin-eosin staining further delineated nuclear and cytoplasmic compartments and supported the morphological observations (Figure 5B). While control cells maintained normal nuclear morphology and homogeneous cytoplasmic appearance, IBB-4-treated cells displayed evident cytoplasmic vacuolization and nuclear condensation (Figure 5B). These findings indicate that IBB-4 induces significant structural alterations in MDA-MB-231 cells that are consistent with treatment-associated cellular stress and cell death-related processes.

IBB-4 modulates mTOR signaling and associated cellular responses in MDA-MB-231 cells

Indole-benzoxazole derivatives are widely recognized as versatile scaffolds in anticancer research due to their ability to modulate diverse metabolic pathways and cellular processes implicated in cancer pathology.[11-16] Our morphological findings suggest that IBB-4 treatment induces cellular stress accompanied by alterations associated with cell death. Previous work by Alagoz et al.[14] demonstrated that benzoxazole derivatives can target mTOR signaling in breast cancer cell lines. Based on this background and considering the observed morphological features, the effect of IBB-4 on mTOR expression was evaluated by IF staining. As shown in Figure 6A, IBB-4 treatment resulted in a significant reduction in mTOR fluorescence intensity compared with that in the control group ($p < 0.0001$), indicating suppression of mTOR expression.

Given the presence of cytoplasmic vacuole-like structures in treated cells, possible involvement of the autophagic pathway was considered. Since the mTOR-autophagy axis plays a central role in regulating metabolic balance in cancer cells, LC3 expression was subsequently assessed.[19] Quantitative analysis of LC3-associated fluorescence intensity did not reveal a statistically significant difference between control and IBB-4-treated cells (Figure 6B). However, qualitative examination of the immunofluorescence images demonstrated notable alterations in LC3 distribution patterns. In control cells, LC3 staining was predominantly diffuse within the cytoplasm. In contrast, a subset of IBB-4-treated cells exhibited a punctate cytoplasmic pattern suggestive of localized LC3 accumulation. Additionally, intensified LC3 immunoreactivity was observed not only in the cytoplasm but also in the nucleus of certain treated cells. Although total fluorescence intensity remained statistically comparable between groups, these spatial redistribution patterns indicate treatment-associated alterations in LC3 localization. Considering the observed suppression of mTOR expression in IBB-4-treated cells, such changes in LC3 distribution may reflect modulation of the mTOR-autophagy axis. However, further functional analyses would be required to confirm this possibility.

Consistent with previous reports indicating that indole-benzoxazole derivatives frequently promote apoptotic responses in cancer cells,[8-16] caspase-3 expression was evaluated to further characterize the mode of cell death induced by IBB-4. Immunofluorescence analysis revealed markedly increased

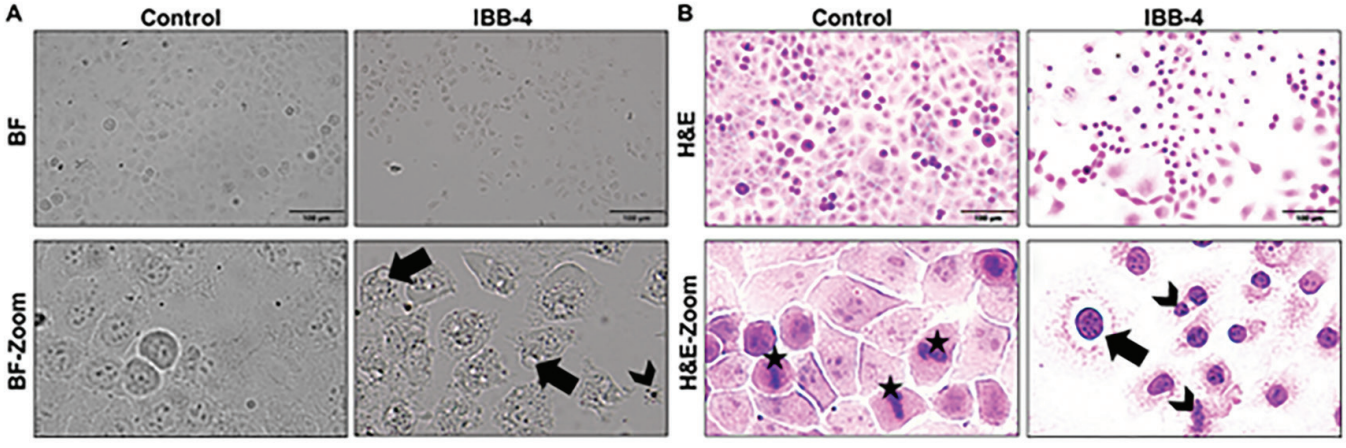


Figure 5. Morphological alterations observed in MDA-MB-231 cells following IBB-4 treatment. A) Representative brightfield microscopy images of control and IBB-4-treated cells. B) H&E-stained images illustrating nuclear and cytoplasmic features. Magnified (zoom) views are shown to highlight morphological changes associated with treatment. Black arrows indicate vacuole-like structures within the cytoplasm. Black arrowheads denote apoptotic cells, and black stars represent mitotic figures. Scale bar: 100 µm.

H&E, hematoxylin and eosin; IBB, indole-benzoxazole derivatives.

caspase-3 immunoreactivity in IBB-4-treated cells compared to controls (Figure 7A). Notably, cells exhibiting reduced size and condensed morphology demonstrated intense caspase-3 staining (Figure 7A). Quantitative fluorescence analysis confirmed a statistically significant elevation in caspase-3 expression following treatment ($p < 0.001$), supporting the involvement of apoptosis-associated mechanisms. Given the pronounced morphological alterations observed upon IBB-4 exposure, the organization of the cytoskeletal network was further examined by assessing β-tubulin distribution. In control cells, β-tubulin displayed a homogeneous, well-organized cytoplasmic distribution, consistent with intact microtubule architecture. In contrast, IBB-4-treated cells exhibited focal accumulation and irregular distribution of β-tubulin, accompanied by disruption of the typical cytoskeletal pattern (Figure 7B). These alterations are consistent with treatment-associated structural reorganization and may reflect cytoskeletal instability accompanying cell death-related processes.

IBB-4 induces spatial reorganization of lipid droplets

Brightfield microscopy revealed notable alterations in cytoplasmic architecture following IBB-4 exposure, including vesicular and clustered structures suggestive of altered lipid droplet organization. Compared with control cells, a subset of IBB-4-treated cells exhibited localized cytoplasmic accumulations confined to discrete regions rather than a diffuse intracellular distribution (Figure 8). Additionally, lipid droplet-like structures were observed in the extracellular space adjacent to certain treated cells. To verify the neutral lipid nature of these structures, ORO staining was performed. In control cells, ORO-positive droplets appeared as small, finely dispersed inclusions with moderate staining intensity and a relatively homogeneous cytoplasmic distribution. In contrast, IBB-4-treated cells demonstrated distinctly bright, intensely red-stained lipid inclusions characterized by dense clusters. These lipid-positive structures were spatially restricted to defined cytoplasmic territories and, in several cells, showed apparent perinuclear enrichment. The overall staining pattern suggested a redistribution of neutral lipid content rather than a uniform increase throughout the cytoplasm (Figure 8).

These findings were further corroborated by Nile red fluorescence analysis. Nile red-positive signals appeared as punctate neutral lipid structures that were more conspicuous and topographically clustered in IBB-4-treated cells than in controls (Figure 8). Consistent with these observations, a three-dimensional surface plot reconstruction generated using ImageJ demonstrated intensified fluorescence peaks that were spatially confined to discrete cytoplasmic regions in IBB-4-treated cells. In contrast, control cells exhibited a more evenly distributed signal pattern (Figure 8).

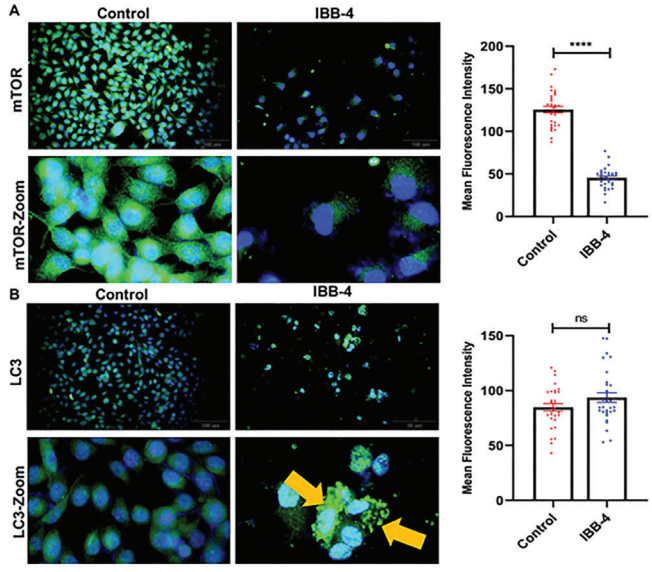


Figure 6. Immunofluorescence analysis of mTOR and LC3 expression in MDA-MB-231 cells following IBB-4 treatment. Representative immunofluorescence images showing mTOR (A) and LC3 (B) expression (FITC, green) in control and IBB-4-treated cells. Nuclei were counterstained with DAPI (blue). Magnified images are provided to highlight localization patterns. Yellow arrows indicate punctate cytoplasmic LC3 staining and nuclear LC3 immunoreactivity observed in IBB-4-treated cells. Quantitative analysis of fluorescence intensity is presented. ****$p < 0.0001$; ns, not significant. Scale bar: 100 µm.

IBB, indole-benzoxazole derivatives.

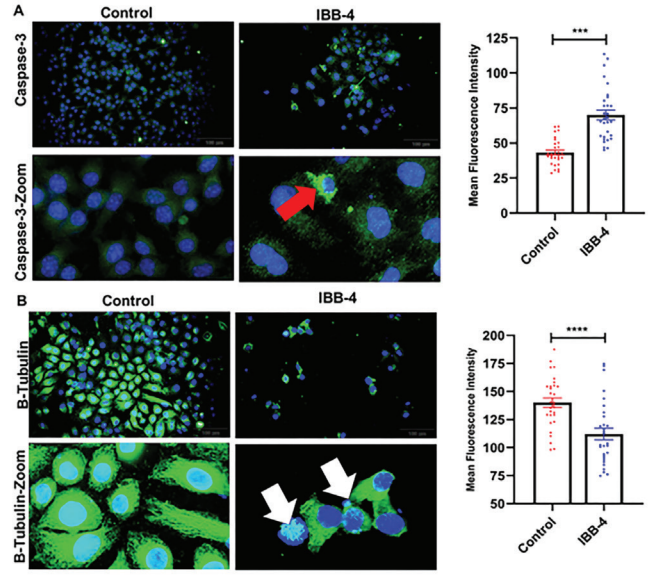


Figure 7. Immunofluorescence analysis of Caspase-3 and β-tubulin expression in MDA-MB-231 cells following IBB-4 treatment. A) Representative immunofluorescence images showing Caspase-3 expression (FITC, green) in control and IBB-4-treated cells. Red arrows indicate Caspase-3-positive cells. B) Immunofluorescence images of β-tubulin expression (FITC, green) illustrating cytoskeletal organization. White arrows denote β-tubulin distribution patterns within the cells. Nuclei were counterstained with DAPI (blue). Enlarged (zoomed) images are provided to highlight localization patterns. A quantitative analysis of fluorescence intensity is presented. ***$p < 0.001$; ****$p < 0.0001$. Scale bar: 100 µm.

IBB, indole-benzoxazole derivatives.

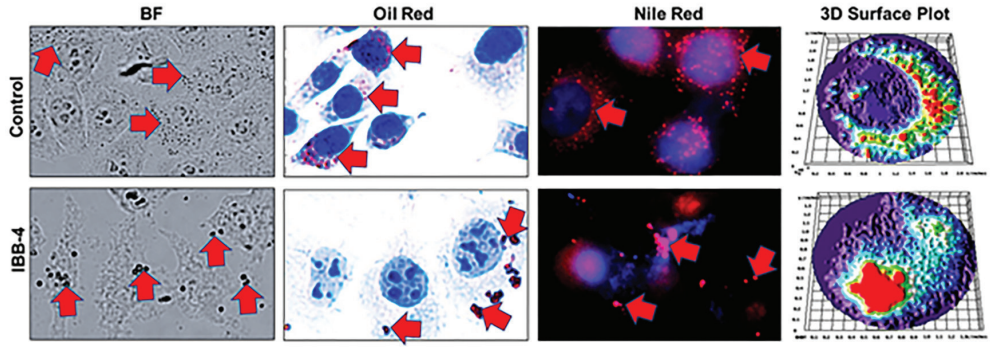


Figure 8. Alterations in lipid droplet distribution following IBB-4 treatment. Representative brightfield images showing lipid droplet-like structures in control and IBB-4-treated cells. Neutral lipid accumulation was assessed by Oil Red O staining (bright red) and confirmed by Nile Red fluorescence analysis. Red arrows indicate lipid droplet structures. A three-dimensional surface plot, reconstructed in ImageJ illustrates the fluorescence intensity distribution within cells. Scale bar: 50 µm.

IBB, indole-benzoxazole derivatives.

DISCUSSION

The present findings show that IBB-4 treatment induces marked changes in the spatial organization and intracellular distribution of neutral lipid droplets. These alterations may reflect changes in cellular lipid homeostasis and may relate to the cellular stress responses associated with IBB-4 exposure. Although the direct effects of benzoxazole derivatives on lipid droplet dynamics have not been extensively explored, previous studies have reported lipid-regulatory effects of certain benzoxazole imine derivatives,[20] while growing evidence supports an important role for lipid droplets in breast cancer biology[18] and cellular stress responses.[17] In this context, the changes observed following IBB-4 treatment may represent an additional cellular response associated with its anticancer activity and may also provide a basis for further investigation of the relationship between lipid droplet remodeling and the biological effects of IBB-4.

Study limitations

The present study has some limitations that should be considered when interpreting the findings. The biological activity of the synthesized compounds was evaluated using *in vitro* breast cancer cell models; therefore, the observed responses may not fully represent the complexity of tumor biology *in vivo*. In addition, the mechanistic evaluation was based primarily on immunofluorescence analysis of selected cellular markers and morphological changes. Although these findings provide useful insights into the cellular effects of IBB-4, a more comprehensive characterization using complementary molecular and biochemical approaches would help clarify the pathways involved. Further studies using appropriate *in vivo* models will be important for evaluating the anticancer activity and pharmacological potential of IBB-4.

CONCLUSION

In this study, a series of indole-benzoxazole hybrid derivatives were synthesized and evaluated for anticancer activity against breast cancer cell lines. Among the tested compounds, IBB-4 showed the strongest activity against MDA-MB-231 cells, with an IC_{50} value of 12.2 µM, and remained highly active against MCF-7 cells, with an IC_{50} value of 12.8 µM. The SAR findings further showed that both the nature and the position of the aromatic substituent influenced cytotoxic activity. In particular, the substantial difference between the methyl-substituted regioisomers IBB-2 and IBB-4 highlights the importance of substituent positioning within this series. IBB-4 also markedly reduced the clonogenic capacity of MDA-MB-231 cells, supporting its strong antiproliferative activity. Further cellular studies demonstrated that IBB-4 affected several aspects of intracellular organization and signaling. Treatment reduced mTOR expression and altered the spatial distribution of LC3, while also increasing caspase-3 immunoreactivity and causing pronounced changes in β-tubulin organization. In addition, IBB-4 caused a marked reorganization and clustering of intracellular neutral lipid droplets, indicating substantial changes in the cellular response to the treatment.

Overall, the findings highlight IBB-4 as a promising member of the indole-benzoxazole series and provide a clear starting point for further structural and biological optimization. The combination of potent cytotoxicity, inhibition of clonogenic growth, and distinct cellular changes observed following treatment supports continued investigation of IBB-4 and related derivatives. Future studies focusing on its molecular targets and activity in more advanced experimental models will help further define the anticancer potential of this scaffold.

Ethics

Ethics Committee Approval: This study does not involve human participants, patient data, or experimental animals. Therefore, ethical approval was not required.

Informed Consent: This study does not involve human participants, patient data, or experimental animals.

Footnotes

Authorship Contributions

Surgical and Medical Practices: B.K., E.A., M.Ç., Concept: B.K., Design: B.K., E.A., Data Collection or Processing: B.K., E.A., M.Ç., Analysis or Interpretation: B.K., E.A., Literature Search: B.K., E.A., Writing: B.K., E.A., M.Ç.

Conflict of Interest: The authors declare no conflicts of interest.

Financial Disclosure: The authors declared that this study received no financial support.

Supplementary Table: https://d2v96fxpocvxx.cloudfront.net/cf9d60d6-523c-458a-a2e6-78728d3ffbb0/content-images/e80e091b-1793-4be2-b585-1a0577a745d1.pdf

REFERENCES

1. Zhang Y, Ji Y, Liu S, Li J, Wu J, Jin Q, Liu X, Duan H, Feng Z, Liu Y, Zhang Y, Lyu Z, Song F, Song F, Yang L, Liu H, Huang Y. Global burden of female breast cancer: new estimates in 2022, temporal trend and future projections up to 2050 based on the latest release from GLOBOCAN. J Natl Cancer Cent. 2025;5:287-296.
2. Devi S. Projected global rise in breast cancer incidence and mortality by 2050. Lancet Oncol. 2025:S1470-2045(25)00136-6.
3. Weigelt B, Geyer FC, Reis-Filho JS. Histological types of breast cancer: how special are they? Mol Oncol. 2010;4:192-208.
4. Moon HR, Ospina-Muñoz N, Noe-Kim V, Yang Y, Elzey BD, Konieczny SF, Han B. Subtype-specific characterization of breast cancer invasion using a microfluidic tumor platform. PLoS One. 2020;15:e0234012.
5. Lehmann BD, Bauer JA, Chen X, Sanders ME, Chakravarthy AB, Shyr Y, Pietenpol JA. Identification of human triple-negative breast cancer subtypes and preclinical models for selection of targeted therapies. J Clin Invest. 2011;121:2750-2767.
6. Xiong X, Zheng LW, Ding Y, Chen YF, Cai YW, Wang LP, Huang L, Liu CC, Shao ZM, Yu KD. Breast cancer: pathogenesis and treatments. Signal Transduct Target Ther. 2025;10:49.
7. Chen R, Zhou Z, Meng X, Lei Y, Wang Y, Wang Y. Emerging opportunities to treat drug-resistant breast cancer: discovery of novel small-molecule inhibitors against different targets. Front Pharmacol. 2025;16:1578342.
8. El-Shoukrofy MS, Amr ME, Okda TM, Omar AME, AboulWafa OM. Novel benzoxazole-based hybrids as multi-target inhibitors of aromatase, EGFR, and PI3K with potential anti-breast cancer activity. Bioorg Med Chem. 2026;133:118477.
9. Omar AME, AboulWafa OM, El-Shoukrofy MS, Amr ME. Benzoxazole derivatives as new generation of anti-breast cancer agents. Bioorg Chem. 2020;96:103593.
10. Omar AME, AboulWafa OM, Amr ME, El-Shoukrofy MS. Antiproliferative activity, enzymatic inhibition and apoptosis-promoting effects of benzoxazole-based hybrids on human breast cancer cells. Bioorg Chem. 2021;109:104752.
11. Mahdi ZH, Alsalim TA, Abdulhussein HA, Majed AA, Abbas S. Synthesis, molecular docking, and anti-breast cancer study of 1-H-indol-3-carbohydrazide and their derivatives. Results Chem. 2024;11:101762.
12. Gaur A, Peerzada MN, Khan NS, Ali I, Azam A. Synthesis and anticancer evaluation of novel indole based arylsulfonylhydrazides against human breast cancer cells. ACS Omega. 2022;7:42036-42043.
13. Singla R, Gupta KB, Upadhyay S, Dhiman M, Jaitak V. Design, synthesis and biological evaluation of novel indole-benzimidazole hybrids targeting estrogen receptor alpha (ER-α). Eur J Med Chem. 2018;146:206-219.
14. Alagoz MA, Resitoglu MT, Kuzu B, Sabrie Z, Yetkin D, Zobi C, Tiftik RN, Firat SS, Gürsoy S, Hepokur C, Algul O. Development of benzoxazole derivatives targeting mTOR: a promising approach for breast cancer therapy. ChemSelect. 2025;10:e01424.
15. Kuzu B, Hepokur C, Turkmenoglu B, Burmaoglu S, Algul O. Design, synthesis and *in vitro* antiproliferation activity of some 2-aryl and -heteroaryl benzoxazole derivatives. Future Med Chem. 2022;14:1027-1048.
16. Kuzu B, Yetkin D, Hepokur C, Algul O. Pyrrole-tethered bisbenzoxazole derivatives: apoptosis-inducing agents targeting breast cancer cells. Chem Biol Drug Des. 2025;105:e70078.
17. Wan M, Pan S, Shan B, Diao H, Jin H, Wang Z, Wang W, Han S, Liu W, He J, Zheng Z, Pan Y, Han X, Zhang J. Lipid metabolic reprograming: the unsung hero in breast cancer progression and tumor microenvironment. Mol Cancer. 2025;24:61.
18. Abramczyk H, Surmacki J, Kopeć M, Olejnik AK, Lubecka-Pietruszewska K, Fabianowska-Majewska K. The role of lipid droplets and adipocytes in cancer. Raman imaging of cell cultures: MCF10A, MCF7, and MDA-MB-231 compared to adipocytes in cancerous human breast tissue. Analyst. 2015;140:2224-2235.
19. Deleyto-Seldas N, Efeyan A. The mTOR-autophagy axis and the control of metabolism. Front Cell Dev Biol. 2021;9:655731.
20. Zaib M, Malik MNH, Shabbir R, Mushtaq MN, Younis W, Jahan S, Ahmed I, Kharl HAA. Imine derivatives of benzoxazole attenuate high-fat diet-induced hyperlipidemia by modulation of lipid-regulating genes. ACS Omega. 2023;8:15306-15317.
21. Malik M, Roy N, Sakkarai Mohamed AP, Lotana H, Shah K, Kumar D. l-Proline catalysed synthesis and *in silico* studies of novel α-cyano bis(indolyl)chalcones as potential anti-cancer agents. RSC Adv. 2025;15:4593-4606.
22. Deniz E, Çöven FO, Ergüç A, Karakuş F, Kuzu B. Design, synthesis, and evaluation of benzoxazole-linked pyrazole hybrids as VEGFR-2-targeted antiproliferative agents. Cell Biochem Biophys. 2025;83:4961-4975.
23. Kuzu B, Cakir M, Acikgoz E. Strategic engineering of imidazopyridine-benzoxazole hybrids targeting microtubule dynamics: comprehensive inhibition of the metastatic cascade. Bioorg Chem. 2026;109615.
24. Cakir M, Kuzu B. Novel Imidazopyridine-oxadiazole β-tubulin inhibitors suppress breast cancer migration and induce caspase-3-mediated apoptosis. ACS Omega. 2026;11:3273-3282.
25. Liu S, Zhang X, Wang W, Li X, Sun X, Zhao Y, Wang Q, Li Y, Hu F, Ren H. Metabolic reprogramming and therapeutic resistance in primary and metastatic breast cancer. Mol Cancer. 2024;23:261.